TABLE I

Resonator	Design Resonant Frequency (GHz)	Actual Resonant Frequency (GHz)	Q	P_L
(1)	20.0	18.920	82	.9641
(2)	20.0	19.194	149	.9667
(3)	16.0	15.41	182	.9850
(4)	12.0	11.505	201	.9850
(5)	20.0	18.885	77	.9619
(6)	20.0	19.173	128	.9613
(7)	16.0	15.342	117	.9745
(8)	20.0	17.897	57	.9195
(9)	8.0	7.522	131	.9773
(10)	16.0	13.457	19	.8641
(11)	20.0	16.406	13	.8144

Resonators

Shielded Lines

(1) #5S 10 mil Duroid
(2) #5L 10 mil Duroid
(3) #4S 10 mil CuFlon
(4) #3S 10 mil CuFlon (short shield)

Unshielded Lines

(5) #5S 10 mil Duroid
(6) #5L 10 mil Duroid
(7) #4S 10 mil Cuflon
(8) #5L 31 mil CuFlon
(9) #2S 31 mil CuFlon
(10) #4S 31 mil CuFlon*
(11) #5S mil Cuflon*

*Low Q caused by poor metallization in the fabrication process.

on Duroid ($\epsilon_r = 2.17$) and CuFlon ($\epsilon_r = 2.1$) substrates of thickness of 10 or 31 mils. The characteristic impedances of all lines was 50 Ω. Table I shows the results obtained for shielded and unshielded resonators, along with the design resonant frequency and calculated Q. The resonators were manufactured by a metalization process and the variation in measured Q for similar resonators is believed to be due to the quality of the metalization. The design and construction of the resonators was carried out at the NASA Lewis Research Center [10] as were the measurements.

The calculated Q's listed in this table are in good agreement with estimated Q's determined from the bandwidth of the $|\Gamma_{in}|^2$ curve at the 6 dB return loss points.

The approach presented here offers several advantages over other techniques commonly used to determine the Q of a microstrip resonator. They are:

1) ρ_L and Q are determined fom the fitted $|\Gamma_{in}|^2$ curve directly.

2) Using seven measured data points allows more of the available information to be used to determine the Q.

3) Curve fitting of the data reduces measurement induced error.

4) A dispersion model is introduced so that the effects of dispersion are included.

5) An accurately established reference plane is not required in making the measurements.

6) No detailed model of the coupling gap is needed. This approach is suitable for analyzing resonators using asymmetric coupling gaps, where $S_{11} \neq S_{22}$, with only slight modification.

References

[1] D. Kajfez and E Hwan, "Q-factor measurements with network analyzer," *IEEE Trans. Microwave Theory Tech.*, vol. 32, pp. 666–670, July 1984.

[2] A. Khanna and Y. Gerault, "Determination of loaded, unloaded, and external quality factors of a dielectric resonator coupled to a microstrip line," *IEEE Trans. Microwave Theory Tech.*, vol. 31, pp. 261–264, Mar. 1983.

[3] R. A. Pucel and D. J. Masse, "Losses in microstrip," *IEEE Trans. Microwave Theory Tech.*, vol. 16, pp. 348–350, June 1968.

[4] E. H. Ginzton, *Microwave Measurements*. New York: McGraw Hill, 1957, pp. 391–434.

[5] P. Silvester and P. Benedek, "Equivalent capacitance of microstrip open circuits," *IEEE Trans. Microwave Theory Tech.*, vol. MTT-20, pp. 511–516, Aug. 1972.

[6] W. J. Getsinger, "Microstrip dispersion model," *IEEE Trans. Microwave Theory Tech.*, vol. 21, pp. 34–39, Jan. 1973.

[7] M. Kobayashi, "A dispersion formula satisfying recent requirements in microstrip CAD," *IEEE Trans. Microwave Theory Tech.*, vol. 36, pp. 1246–1250, Aug. 1988.

[8] P. Benedek and P. Silvester, "Equivalent capacitance of microstrip gaps and steps," *IEEE Trans. Microwave Theory Tech.*, vol. 20, pp. 729–733, Nov. 1972.

[9] K. C. Gupta, R. Garg, and I. J. Bahl, *Microstrip Lines and Slotlines*. Dedham Mass.: Artech House, 1979, pp. 130–136.

[10] R. R. Romanofski, *et al.* "An experimental investigation of microstrip properties on soft substrates from 2 to 40 GHz," in *1985 IEEE MTT-S International Microwave Symposium Dig.*, St. Louis, MO, 1985, pp. 675–678.

Conformal Mapping Analyses of Microstrips with Circular and Elliptical Cross-Sections

M. A. Martens, R. W. Brown, and E. M. Haacke

***Abstract*—A new conformal transformation is derived in terms of a Schwarz–Christoffel transformation involving elliptic integrals of the first and third kind. This mapping function is used to give exact solutions for TEM excitations of microstrips and coupled microstrips with circular and elliptical cross-sections. Using these maps, the uniformity of the TEM mode magnetic field inside an elliptical slotted tube transmission line is investigated.**

I. Introduction

Due to the interest in nonplanar microstriplines with circular and elliptical cross-sections [1]–[7] it is certainly useful if one can find an analytic solution for the fields produced in these geometries. Some of the methods suggested in the literature involve either infinite series [1], [3], [7] or iterations [5]. In contrast to these methods, the conformal mapping technique, if successful, provides an exact closed-form solution. Although conformal mapping has been applied to this class of problems [2], [4], [6], the geometries are mapped into a finite region of a domain where the conductors are planar and then one or more of the transverse dimensions of the conductors are assumed to extend to infinity.

It is the purpose of this paper to present a complete set of conformal transformations that are used to analyze the TEM modes of the circular and elliptical geometries shown in Fig. 1. No assump-

Manuscript received June 18, 1991; revised February 7, 1992. This work was supported by the Whitaker Foundation and by Picker International.

M. A. Martens was with the Department of Physics, Case Western Reserve University, Cleveland, OH 44106. He is presently with Fermi National Accelerator Laboratory, Batavia, IL 60510.

R. W. Brown is with the Department of Physics, Case Western Reserve University, Cleveland, OH 44106.

E. M. Haacke is with the Department of Physics, Case Western University, Cleveland, OH 44106. He is also with the Radiology Department, University Hospitals of Cleveland.

IEEE Log Number 9201725.

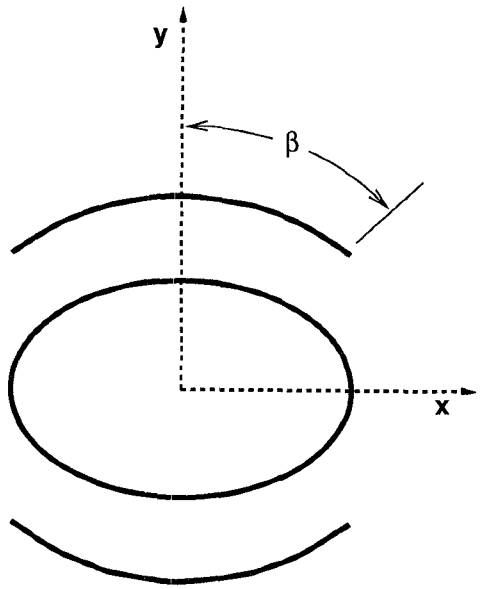

Fig. 1. Elliptical geometry. The inner elliptical cylinder has an eccentricity ϵ_g and is at potential $\Phi = 0$. The outer elliptical arcs lie on an ellipse with eccentricity ϵ_c. For the elliptical coupled microstrips, the upper arc is at potential $\Phi = 1$ while the lower arc is at $\Phi = \pm 1$. For the elliptical microstriplines the lower arc is absent. The circular geometries are similar to the elliptical geometries (the inner cylinder becomes circular with a radius r_g and the outer arcs lie on a circle of radius r_c) except that the arcs may lie either inside or outside the grounded cylinder.

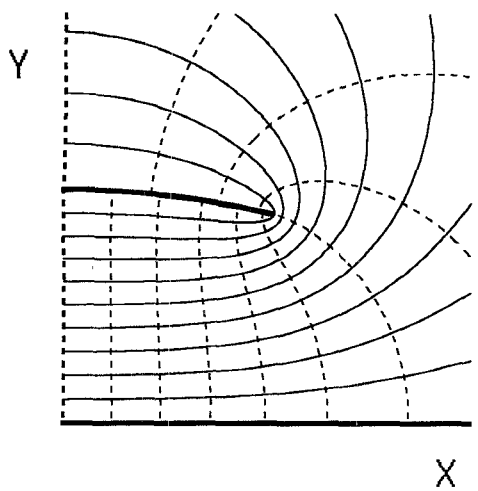

Fig. 2. One quadrant of the elliptical slotted tube transmission line. The outer elliptical arc is at potential $\Phi = 1$. By symmetry, the y axis is a streamline and the x axis is at $\Phi = 0$. (The solid (dashed) lines represent equipotential lines (streamlines).

tion is made about an infinite extension of any segment in the cross section. To accomplish this, a new transformation involving incomplete elliptic integrals of the first and third kind is derived. This new mapping, along with other familiar mapping functions, provides a means of transforming the problematic geometries into a region where the complex potential can be found by inspection.

There is also interest in the use of slotted tube resonators (STR) in Nuclear Magnetic Resonance (NMR) applications [8]. The STR is part of an rf system that provides a sinusoidally time varying magnetic field with a spatially uniform magnitude. The degree of uniformity of this magnetic field is important since the spatial variation is a key to understanding image response. It is, therefore,

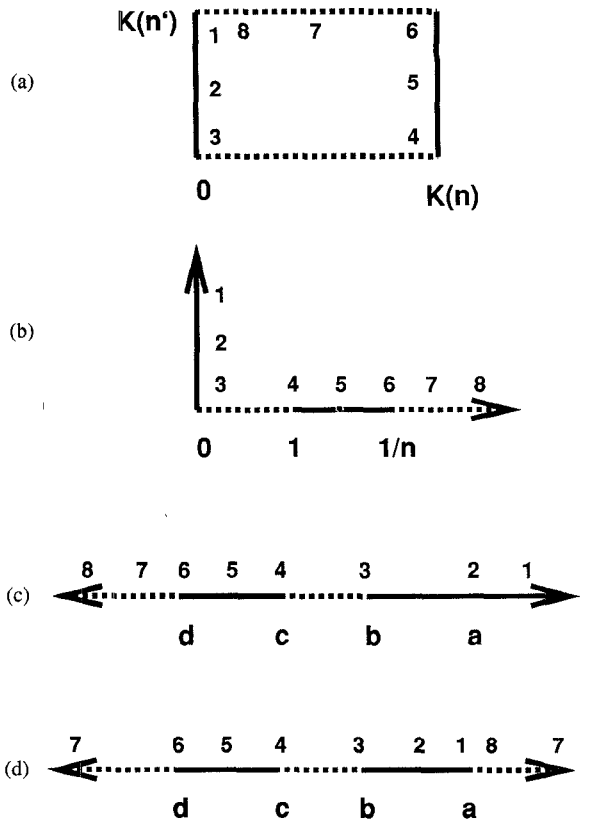

Fig. 3. Initial regions in the mapping sequence. Solid (dashed) lines represent equipotential (stream) lines. (a) The w-plane. The rectangular region is bounded by two lines at potential $\Phi = 0$ and $\Phi = 1$ and two streamlines. (b) The ζ-plane. Region consists of upper right quadrant. (c) The t_o-plane. Region consists of upper half-plane. (d) The t_e-plane. Region consists of upper half-plane.

useful to find an analytical solution for the magnetic field profile. In [8], an STR with circular geometry is considered. By using an STR with elliptical rather than circular cross-section, it is possible to improve the uniformity of the field. Using the same conformal maps developed for the striplines, we solve for the TEM fields of the elliptical STR shown in Fig. 2. Using these solutions we investigate the uniformity of the magnetic field as a function of eccentricity and conductor angle.

II. Common Transformations

To discuss the transformations necessary to map the sequence of regions shown in Fig. 3, four real parameters a, b, c, and d are introduced and related to the geometries later. The starting region is the rectangular portion of the w-plane shown in Fig. 3(a). $K(n)$ and $K(n')$ are complete elliptic integrals of the first kind [9] with parameters $n^2 = (b - c)/(b - d)$ and $n'^2 = 1 - n^2$. The two sides of the rectangle at 0 and $K(n)$ have potentials $\Phi = 0$ and $\Phi = 1$ while the top and bottom are Neumann boundaries. By inspection, we see that the complex potential in the w-plane is given by $\Omega = \Phi + i\Psi = w/K(n)$ where lines with constant $\Phi(\Psi)$ are equipotential (streamlines).

The first transformation in the mapping sequence is the familiar Jacobi elliptic function [10] $\zeta = \mathrm{sn}\,(w, n)$, which maps the region in the w-plane to the upper right quadrant of the ζ-plane shown in Fig. 3(b).

At this point, the mapping sequence splits into two directions with the final geometry deciding which path is chosen. These two

branches are labeled the even and odd modes for reasons that become obvious later in the paper.

For the odd mode, the simple transformation $t_o = b - (b - c)[\zeta^*]^2$ maps the ζ-quadrant into the upper half of the t_o-plane shown in Fig. 3(c).

For the even mode, the mapping sequence starts in the w-plane and uses the $\zeta = \text{sn}(w, n)$ transform as before, but in this case $n = (b' - c')/(b' - d')$ where

$$b' = \frac{b(a-d)}{(a-b)}, \quad c' = \frac{c(a-d)}{(a-c)}, \quad d' = d. \tag{1}$$

The simple transformation $t' = b' - (b' - c')[\zeta^*]^2$ then maps the ζ-quadrant into the upper half of the t'-plane. (The t'-plane is not shown but is the same as the t_o-plane shown in Fig. 3(c) with a, b, c, d replaced by a', b', c', d'.)

The bilinear transform

$$t_e = \frac{at'}{t' - d + a} \tag{2}$$

is used next to map the upper half of the t'-plane into the upper half of the t_e-plane shown in Fig. 3(d). The purpose of this transformation is to map the Dirichlet boundary condition from b' to $+\infty$ in the t'-plane onto the line segment from b to a in the t_e-plane. As a result, the segment from a to $+\infty$ in the t_e-plane becomes a streamline or Neumann boundary condition.

III. Schwarz–Christoffel Transform

The transformation developed here, a special case of the Schwarz–Christoffel transformation [10], maps the $t_{e,o}$-plane onto a semi-infinite strip in the $f_{e,o}$-plane. For our particular case the mapping function is given by

$$f_{e,o} = \frac{1}{2}\int_b^t \frac{t\,dt}{\sqrt{(a-t)(t-b)(t-c)(t-d)}} \tag{3}$$

where t is either t_o or t_e. Note that the segment from a to ∞ is mapped to the line $\text{Re}\{f_{e,o}\} = \pi/2$.

By making the substitution [9]

$$\vartheta = \phi + i\psi = \sin^{-1}\sqrt{\frac{(a-c)(t-b)}{(a-b)(t-c)}} \tag{4}$$

equation (3) can be expressed as

$$f = \frac{b}{\alpha^2}[(\alpha^2 - \alpha_1^2)\Pi(\vartheta, \alpha^2, k) + \alpha^2 F(\vartheta, k)] \tag{5}$$

where

$$k^2 = \frac{(a-b)(c-d)}{(a-c)(b-d)} \tag{6}$$

$$\alpha^2 = \frac{(a-b)}{(a-c)} \tag{7}$$

$$\alpha_1^2 = \frac{c(a-b)}{b(a-c)} \tag{8}$$

and $F(\vartheta, k)$ and $\Pi(\vartheta, \alpha^2, k)$ are incomplete elliptic functions of the first and third kind. Because ϑ is complex, these functions are complex in general. Using relations from [9] and [11], we can separate elliptic integrals of complex argument into real and imaginary parts.

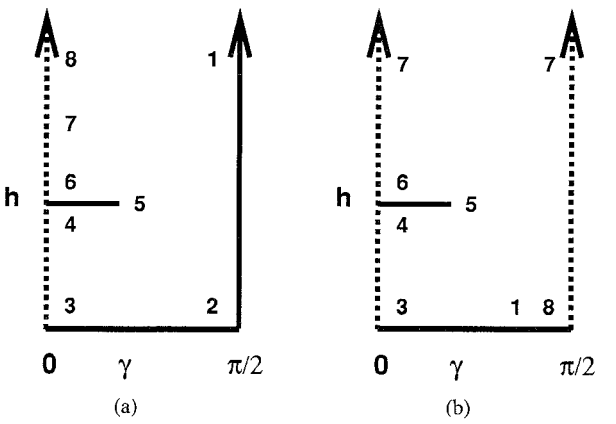

Fig. 4 f-plane. (a) f_o-plane. The left side is a streamline, the segment at h is at potential $\Phi = 1$, and the bottom and right side are at potential $\Phi = 0$. (b) f_e-plane. Same as f_o-plane exept that the right is a streamline.

The result is

$$F(\vartheta, k) = F(\theta, k) + iF(\mu, k') \tag{9}$$

$$\Pi(\vartheta, \alpha^2, k) = \Pi(\theta, \alpha^2, k) + i\frac{1}{1-\alpha^2} \cdot [F(\mu, k') - \alpha^2\Pi(\mu, 1-\alpha^2, k')] - \frac{\alpha^2}{\lambda}\tan^{-1}\Gamma \tag{10}$$

where

$$k'^2 = (1 - k^2)$$

$$\lambda^2 = \alpha^2(1-\alpha^2)(\alpha^2 - k^2) \tag{11}$$

$$\Gamma = \frac{i\lambda \sin\theta \tan\mu \sin\vartheta}{1 - \alpha^2\sin^2\vartheta + i\alpha^2 \sin\theta\tan\mu\cos\vartheta\sqrt{1-k^2\sin^2\vartheta}}. \tag{12}$$

and the real angles θ and μ are determined as follows: $x = \cot^2\theta$ is the positive root of

$$x^2 - [\cot^2\phi + k^2\sinh^2\psi\csc^2\phi - k'^2]x - k'^2\cot^2\phi = 0 \tag{13}$$

and then μ comes from

$$k^2\tan^2\mu = \tan^2\phi\cot^2\theta - 1. \tag{14}$$

Using [9] the parameters a, b, c, and d can be related to geometry of the f-plane via the following equations,

$$(a-c)(b-d) = 1 \tag{15}$$

$$(b-c)\Pi(\alpha^2, k) + cK(k) = \pi/2 \tag{16}$$

$$(b-a)\Pi(1-\alpha^2, k'), + aK(k') = h \tag{17}$$

$$(b-c)\Pi(\theta', \alpha^2, k) + cF(\theta', k) - \tan^{-1}\left(\frac{bc}{-ad}\right) = \gamma \tag{18}$$

with

$$\theta' = \sin^{-1}\sqrt{\frac{c(b-d)}{b(c-d)}} \tag{19}$$

where h and γ are as shown in Fig. 4.

IV. Circular Geometry

The mapping sequences for the circular geometries are completed by using the exponential function. Due to the symmetry of the geometries considered it is necessary to map only one half or one quarter of the plane. In all of the cases considered the y-axis of Fig. 1 is a streamline and the coupled microstrip geometries have additional symmetry about the x-axis.

Microstrip: The transformation for the circular microstripline (Fig. 1 without the lower circular arc), is given by $z = e^{-i(2f_e - \pi/2)}$. This transformation maps lines of constant Im $\{f_e\}$ onto circular arcs and lines of constant Re $\{f_e\}$ onto radial lines. Thus, in the z-plane, the radius of the grounded cylinder is 1, the half-angle of the outer condition is $\beta = 2\gamma$, and the radius of the outer conductor is $r_c = e^{2h}$. In this case only one half of the z-plane is mapped.

Coupled Microstrips: For the circular coupled microstrips (Fig. 1), the map is given by $z = e^{-i(f_{e,o} - \pi/2)}$ where the even and odd TEM modes are mapped using the f_e- and f_o-planes, respectively. The radius of the grounded cylinder is 1, $\beta = \gamma$, and $r_c = e^h$.

Shielded Transmission Line: For the shielded circular transmission line (Fig. 1 with $r_c < r_g$) the map is given by $z = e^{i(f_{e,o} - \pi/2)}$. This map is similar to the coupled microstrip case except that the circular arcs are now inside the grounded cylinder. The even and odd TEM modes are mapped using the f_e and f_o-planes, respectively. The radius of the grounded cylinder is 1, $\beta = \gamma$, and $r_c = e^{-h}$.

V. Elliptical Geometry

The elliptical geometries are mapped using the sine function and, as in the circular case, we use the symmetry of the problem and map only one half or one quarter of the plane. Note that there is no solution for the elliptical shielded transmission line.

Microstrip: The elliptical microstripline shown (Fig. 1 without the lower elliptical arc) is mapped via $z = \sin[2(f_e + ig)]$. This transformation maps lines of constant Im $\{f_e\}$ onto ellipses and lines of constant Re $\{f_e\}$ onto hyperbolae. The parameters h, g, and γ are related to the eccentricity of the inner ellipse, $\epsilon_g = \text{sech}(2g)$, the eccentricity of the conductor, $\epsilon_c = \text{sech}(2(g + h))$, and the conductor half-angle, $\tan\beta = \sqrt{1 - \epsilon_c^2}\tan(2\gamma)$.

Coupled Microstrips: For the coupled microstrips (Fig. 1) the map is $z = \sin[(f_{e,o} + ig)]$ where the even and odd TEM modes are mapped using f_e- and f_o-plane, respectively. The eccentricities and the angles are related as above without the factors of 2. A special case of this map, using the f_o-plane and $g = 0$, is the elliptical slotted tube shown in Fig. 2.

VI. Capacitance of Microstrips

Since the capacitance and inductance per unit length do not change under a conformal mapping transformation, these quantities are calculated in the w-plane. The capacitance is given simply by $C = \epsilon K(n')/K(n)$ and the inductance by $L = \mu K(n)/K(n')$ where the value of the parameter n depends on the geometry of interest. For a particular geometry, h and γ easily determined. The set of four equations 15–18 are then used to solve for the four parameters a, b, c, and d (and therefore n).

Using a computer to numerically solve these equations, we were able to find solutions for the cases in which $h > 0.1$. However, as h becomes small (<0.1) it becomes difficult to numerically solve this set of equations. The difficulty is caused by the singularity in the elliptic integral of the third kind as α^2 approaches 1. The case in which h becomes small corresponds to microstrips in which the conducting strip is relatively close to the inner grounded cylinder. The capacitance calculations for these cases are handled accurately by the works of the authors mentioned in the introduction.

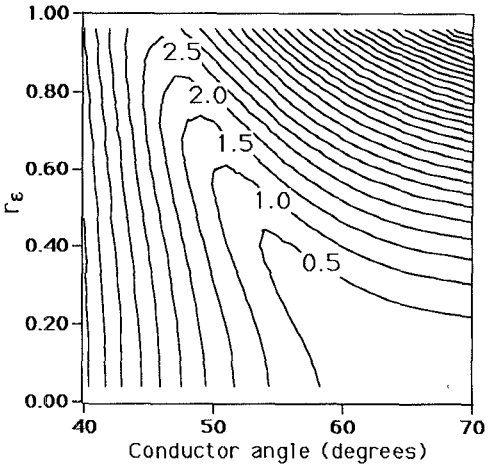

Fig. 5. MSE × 100 for a circular region with a radius of 0.6. Left axis is r_ϵ and the bottom axis is the conductor angle γ.

VII. Uniformity of STR

We now return to the problem of maximizing the uniformity of the magnetic field inside an STR. We are interested in the magnetic field in some region inside of the elliptical slotted tube in Fig. 2. To quantify the uniformity we use the mean square error (MSE) as defined by

$$MSE = \frac{1}{B_o}\sqrt{\frac{1}{A}\int\int |\vec{B} - \vec{B}_o|^2\, da} \tag{20}$$

where $\vec{B}_o = B_o\hat{x} = \vec{B}(\vec{r} = 0)$ is the ideal uniform field, and A is the area of the region integrated over.

Given a fixed region of interest we wish to find the eccentricity and angle that minimize the MSE. As an example this calculation is done using a circular region with a radius of 0.6. The minor radius of the elliptical conductor was fixed at 1 while the conductor angle and the ratio of the minor axis to the major axis (r_ϵ) were varied. The results of this calculation are shown in Fig. 5.

As is seen in this plot, the flatter and wider the conductors become, the lower the MSE. Since it is impractical to have infinitely wide conductors some limits must be placed on the widths of the conductors. Consider, for instance, constraining the conductor to a half-width of 1 in the x direction. In this case the circular region has a minimum MSE of 0.0092 when the elliptical conductor has $\gamma = 50.7°$ and $r_\epsilon = 0.58$ (or eccentricity = 0.81). As a comparison, a circular conductor with $\gamma = 45°$ has an MSE of 0.029 and a set of parallel plates with half-width of 1 has an MSE of 0.033.

Acknowledgment

We are grateful to John Patrick, Dee Wu, and Labros Petropoulos for their help.

References

[1] Y. C. Wang, "Cylindrical and cylindrically warped strip and micostriplines," *IEEE Trans. Microwave Theory Tech.*, vol. MTT-26, pp. 20–23, Jan. 1978.

[2] K. K. Joshi, M. E. Rao, and B. N. Das, "Characteristic impedance of nonplanar striplines," *Proc. Inst. Elec. Eng.*, pt H, vol. 127, no. 5, pp. 287–291, Oct. 1980.
[3] B. N. Das, A. Chakrabarty, and K. K. Joshi, "Characteristic impedance of elliptic cylindrical strip and microstriplines filled with layered substrate," *Proc. Inst. Elec. Eng.*, pt H, vol. 130, no. 4, pp. 245–250, June 1983.
[4] L. R. Zeng and Y. X. Wang, "Accurate solutions of elliptical and cylindrical striplines and microstrip lines," *IEEE Trans. Microwave Theory Tech.*, vol. MTT-34, pp. 259–265, Feb. 1986.
[5] C. H. Chan and R. Mittra, "Analysis of a class of cylindrical multiconductor transmission lines using an iterative approach," *IEEE Trans. Microwave Theory Tech.*, vol. MTT-35, pp. 415–423, Apr. 1987.
[6] C. J. Reddy and M. D. Deshpande, "Characteristics of inhomogeneous coupled cylindrical striplines," *Electron. Lett.*, vol. 23, no. 16, pp. 821–822, July 1987.
[7] M. D. Deshpande and C. J. Reddy, "Spectral-domain analysis of single and coupled cylindrical stripline," *IEEE Trans. Microwave Theory Tech.*, vol. MTT-35, pp. 672–675, July 1987.
[8] H. J. Schneider and P. Dullenkopf, "Slotted tube resonator: A new NMR probe head at high observing frequencies," *Rev. Sci. Instrum.*, vol. 48, no. 1, pp. 68–73, Jan. 1977.
[9] P. F. Byrd and M. D. Friedman, "Formulae 116.01, 116.02, 161.02, and 256.11" in *Handbook of Elliptic Integrals for Engineers and Scientists*. New York: Springer, 1971.
[10] G. F. Carrier, M. Krook, C. E. Pearson, Section 4.4 of *Functions of a Complex Variable*. New York: McGraw-Hill, 1966.
[11] M. Abramowitz and I. A. Stegun, Section 17.4.11 of *Handbook of Mathematical Functions (Applied Mathematics Series 55)*, National Bureau of Standards, 1970.

Analysis of an N-Port Consisting of a Radial Cavity and E-Plane Coupled Rectangular Waveguides

Marek E. Bialkowski

***Abstract*—An analysis of an n-port including a radial or coaxial cavity and E-plane coupled rectangular waveguides is presented. A nonstandard field matching technique which exploits both circular and rectangular boundaries, is used to determine the scattering matrix parameters of the n-port. Validity of the analysis is verified through comparison with an alternative analysis and experiment.**

Introduction

Microwave networks consisting of a number of rectangular waveguides coupled in the E-plane to a radial or coaxial cavity find many useful applications in microwave engineering. A well known rat-race circuit consisting of four waveguides coupled to a coaxial cavity is a typical example.

Recently, some interest has been shown in E-plane coupled waveguide five ports [1]–[4]. It has been demonstrated that these five-ports can be used as power combiners [4] or as building blocks for six-port network analysers [1], [3].

So far, the design of E-plane coupled waveguide n-ports has been based on experiment (i.e. [1], [4]). The only theoretical analysis of an E-plane waveguide n-port has been presented in [2]. The analysis was restricted to the symmetrical five-port junction and was based on the least-squares boundary residual method (LSBRM). A good agreement with experiment was noted.

In order to set equations for unknown modal expansion coefficients the authors in [1] used the continuity conditions for tangential components of the fields only along the circular contour of the cavity. Since equations for unknown expansion coefficients for the cavity region were inseparable from those of the rectangular waveguide region, the size of the resulting matrix was large.

In this paper an alternative analysis based on a field matching technique for an E-plane n-port is described. In difference to the method presented in [1] both rectangular and circular boundaries are exploited in setting up the continuity conditions for the tangential field components. This approach leads to separation of modal expansion coefficients for the waveguide region from those of the cavity region. In this way a considerable reduction of the size of the matrix involved in solving equations for unknown modal expansion coefficients is achieved.

The solution presented here exhibits good convergence and is easily implemented on an IBM PC or compatible.

Analysis

The structure of the analyzed n-port circuit is shown in Fig. 1.

The n-port consists of N radially positioned rectangular waveguides which are connected in the E-plane to a radial or coaxial cavity. The positions of the rectangular guides with respect to the radial or coaxial cavity are given by angles Φ_i, $i = 1, \cdots, N$.

From the designers point of view, the parameters of interest are the scattering matrix coefficients of the n-port.

Assuming dominant mode operation of the individual waveguides, the determination of the scattering parameters requires the n-times solving of an electromagnetic problem, in which one of the waveguides is connected to the generator and the remaining waveguides are match-terminated. There are a number of ways to solve this formulated EM problem. The method chosen here is based on the non-standard field matching technique which exploits both circular and rectangular natural boundaries, associated with the geometry of the N-port.

Field Matching Solution

It is sufficient to present the method for the case when waveguide No. 1 is excited and the remaining waveguides are match-terminated.

Under the condition of the dominant mode operation, the rectangular waveguides support free propagation of the TE_{10} mode. The other modes are excited at the inter-junctions between rectangular waveguides and the cavity, but quickly decay over distance. Due to the form of excitation the waveguide and cavity modes combine in such a way that the y-component of the electric field is zero. In this case the total field in all the regions of the n-port can be considered as the radial TE. Its components can be derived from the knowledge of the y-component of the magnetic field.

The y-component of the magnetic field in the waveguides can be written in the Cartesian system of coordinates in the form (1):

$$H_y^l = \frac{-j\Gamma_1^2}{kZ}\left[\frac{e^{-\Gamma_{01}z}}{\Gamma_{01}}\delta_{1i} - \sum_{m=0}^{\infty} A_{im}\cos(k_{xm}x)\frac{e^{\Gamma_{mi}z}}{\Gamma_{mi}}\right]\sin(k_{y1}y) \quad (1)$$

Manuscript received May 14, 1991; revised February 4, 1992.
The author is with the Department of Electrical Engineering, The University of Queensland, Queensland 4072, Australia.
IEEE Log Number 9201726.